

Zinc oxide and related compounds: order within the disorder

R. Martins, L. Pereira, P. Barquinha, I. Ferreira, R. Prabakaran, G. Gonçalves, A. Gonçalves, E. Fortunato

Materials Science Department, CENIMAT/I3N, Faculty of Science and Technology of New University of Lisbon and CEMOP/UNINOVA, Campus de Caparica, 2829-516 Caparica, Portugal

ABSTRACT

This paper discusses the effect of order and disorder on the electrical and optical performance of ionic oxide semiconductors based on zinc oxide. These materials are used as active thin films in electronic devices such as pn heterojunction solar cells and thin-film transistors. Considering the expected conduction mechanism in ordered and disordered semiconductors the role of the spherical symmetry of the s electron conduction bands will be analyzed and compared to covalent semiconductors. The obtained results show p-type c-Si/a-IZO/poly-ZGO solar cells exhibiting efficiencies above 14% in device areas of about 2.34 cm². Amorphous oxide TFTs based on the Ga-Zn-Sn-O system demonstrate superior performance than the polycrystalline TFTs based on ZnO, translated by I_{ON}/I_{OFF} ratio exceeding 10⁷, turn-on voltage below 1-2 V and saturation mobility above 25 cm²/Vs. Apart from that, preliminary data on p-type oxide TFT based on the Zn-Cu-O system will also be presented.

Keywords: oxide semiconductors, thin film transistors; ordered and disordered semiconductors; solar cells.

1. INTRODUCTION

N-type oxide semiconductors have been extensively used as transparent conductive electrodes for display and solar cells applications^[1-3] where the most used oxides are based on indium tin oxide alloys (ITO), due to the high transmittance in the visible range of the solar spectrum and the low sheet resistance^[4-7]. Due to cost increase of indium and the need to have films able to sustain a hydrogen plasma discharge during the deposition process^[8], zinc aluminum oxide (ZAO)^[9-13] and zinc gallium oxide (ZGO) have been developed as a promising alternative to ITO, since zinc is a quite abundant (about 10³ more than In, as taken from *www.environmentalchemistry.com*) and “green” material. Besides that, gallium has a better doping efficiency than aluminum, allowing room temperature processing^[12, 14, 15]. For these films, the conductivity improvement has been associated with the crystal order and corresponding grain size. Recently, it has also been realized that disordered oxide semiconductors can present excellent optical and electrical properties, namely high conductivity and high mobility, even when processed at room temperature, compatible with the use of flexible substrates^[16, 17].

The use of n-type oxide semiconductors in active electronic functions has been also demonstrated in the last 5-8 years^[18-20], even when produced at room temperature^[21, 22], which extends their ability to be processed on other type of substrates, such as paper^[23-27]. Nowadays these active oxides are key components in a wide range of device applications like sensors^[28] and thin-film transistors (TFTs), where it has been demonstrated that they can present high electronic performance even when disordered ionic oxides are used^[29-34]. Concerning p-type oxide semiconductors, this activity has been also pursued in the last years^[35-43]. Recently, a p-type TFT based on low band gap SnO has been reported^[44], in spite of the difficulty in having metals with a high work function, that are able to perform the required ohmic contact with the p-type oxide with a low carrier concentration (below 10¹⁶ carriers/cm³)^[3, 45].

When comparing the electronic performance of the oxides mentioned above with the one of covalent semiconductors, we observe huge differences, either concerning the doping effect or the role of disorder and order on the materials and devices' properties^[46, 47]. In fact, in covalent semiconductors, the electronic doping effect is mainly related to the substitution of atoms in a matrix (host) by an impurity, which may have a deficit or an excess of valence electrons relatively to the host atoms, leading to a negative or positive charge impurity, to each is connected the existence of an excess of free holes (p-type), or of free electrons (n-type), respectively^[48]. The n-doping effect in oxide semiconductors is essentially related to the existence of oxygen vacancies (meaning that the films are non stoichiometric and so there are not enough anions to compensate the existing cations), which work as a source for electrons. Their control depends on

the oxidation state of the cation, which leads to changes in the film composition, as opposed to the substitutional doping in covalent semiconductors [17, 28]. For p-type oxides, a passivation of vacancies and deep defects is also necessary prior to the introduction of the correct impurities in the host matrix [37]. In covalent semiconductors disorder leads to a continuous distribution of localized states, between the edges of the conduction and valence bands. This leads to a strong decrease (several orders of magnitude) of the carriers' mobility [49]. For oxides based in heavy metal cations, this is not the case. Disorder does not lead to the existence of a full carrier's localization and so carrier's mobility is not strongly affected, as it happens in covalent semiconductors [50-52].

In this paper we report on the optical and electrical performance of materials and devices based on ordered and disordered Zinc Oxide (ZnO) and Zinc Gallium Oxide (ZGO), without and with tin (Sn) in its composition (ZGSO). Besides that, a first attempt to produce a p-type TFT based on wide band gap oxide semiconductors will also be reported.

2. EXPERIMENTAL DETAILS

The ZnO, ZGO and ZGSO films were produced by rf magnetron sputtering using a single 3 inches diameter ZnO or ZnO:Ga₂O₃ (95:5 wt%) ceramic target or by co-sputtering, using the ZnO:Ga₂O₃ target and a 2 inches diameter Sn target, (see fig. 1) always with a base pressure below 3×10^{-4} Pa. Other deposition parameters were adjusted as described elsewhere [14, 53].

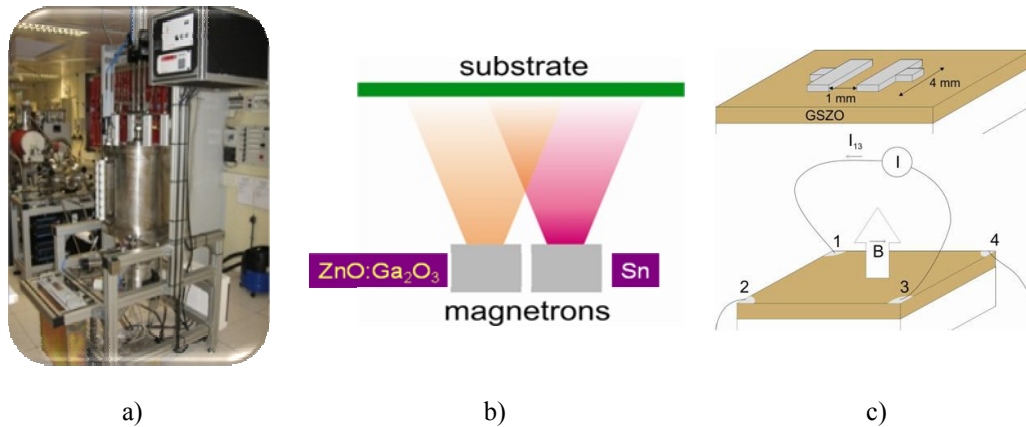


Fig. 1. a) A view of the apparatus and the clean room where the oxide materials and the devices were processed; b) a sketch of the co-sputtering process, allowing to analyze in the same run changes in the films' composition (film close to the right size is Sn rich, while the opposite occurs on the left side); c) electrical testing structures used to determine the films' conductivity as a function of temperature and for hall effect measurements.

To produce the pn heterojunction solar cells, doped p-type crystalline silicon substrates (p-type c-Si, 2.5×2.5 cm in size), 150 μm thick and with an acceptor concentration in the range of $5-10 \times 10^{16}$ at.cm⁻³ were used. The polished surfaces of the crystalline silicon substrate were cleaned (etching the native oxide with a buffered HF solution) and properly rinsed prior to the deposition of the back metal contact by e-beam evaporation, composed by a double layer of silver and chromium (Ag/Cr), 200 nm thick. The n-type polycrystalline ZGO, 100-200 nm thick, was deposited at room temperature (R.T.) by r.f. magnetron sputtering on the opposite side of the substrate, showing a resistivity (ρ) below 7×10^{-4} Ω.cm. In selected devices, a 5-10 nm n-type interlayer based on amorphous indium zinc oxide (a-IZO) with a resistivity in the range of $7-1 \times 10^{-4}$ Ω.cm was deposited, using the conditions described elsewhere [54, 55]. The front metal grid contact was based on Cr/Ag, also deposited by e-beam evaporation. The entire device (with or without the front metal electrode) was annealed in N₂/H₂ (95/5) atmosphere for 30 minutes at 150 and 250 °C, respectively.

The ZnO and ZGSO bottom-gate n-type TFTs were produced using heavily doped p-type c-Si substrates coated with 100 nm thick thermally grown SiO₂, which acts as the gate dielectric, leading to a gate leakage current (I_G) below 10 pA for all the produced devices. Si was simultaneously used as the substrate and the common gate of the devices. A 5/75 nm thick Ti/Au film was deposited by e-beam evaporation on the backside of Si (after etching the backside SiO₂ with a buffered HF solution) to form the gate electrode. A 30-60 nm thick polycrystalline ZnO or amorphous ZGSO (a-ZGSO) layer (the semiconductor) was then deposited by r.f. magnetron sputtering in an Ar/O₂ atmosphere. In the co-sputtering case, the rf power density ratio applied to the ZGO and to the Sn targets was kept around 1.7. The 200 nm thick

source/drain electrodes (Ti) were e-beam evaporated at a rate of 2 Å/s on top of ZnO or a-ZGSO. Both the semiconductor and the source/drain layers were patterned by lift-off and the produced transistors had a fixed width (W) of 50 μm and length (L) of 50 μm. Two different series of a-ZGSO transistors, S1 and S2, were produced: in S1, the a-ZGSO was produced at room temperature, while in S2 it was deposited at 150 °C. After production, both series of TFTs were annealed in a Barnstead Thermolyne F21130 tubular furnace, with a constant flow of nitrogen, at 150, 200, 250 and 300 °C for 1 hour. The first attempts to produce p-type TFT involved the co-sputtering of ZnO and Cu (ZCO) at 150 °C, using an rf power ratio between targets of 1.2. After processing, the films were annealed up to 350°C. The other procedures were similar to the ones already described for the ZnO and ZGSO TFT.

The films' thicknesses were measured with a surface profilometer Sloan Tech Dektak 3. X-ray diffraction measurements were performed at RT in air, using the CuKα line ($\lambda=1.5418 \text{ \AA}$) of a Siemens D-500 diffractometer. The scanning electron microscopy (SEM) analysis was done in a FEI Strata 235-Dual Beam FIB (both in surface and cross section after vertical milling using Ga ions). Atomic force microscopy (AFM) images were also taken for the same set of films, using an Asylum AFM. X-ray Photoelectron Spectroscopy (XPS) analysis was performed using the Al Kα (non monochromatic) radiation of an XSAM800 (KRATOS) spectrometer operated in the fixed analyzer transmission (FAT) with a power of 120 W (10 mA and 12 kV) in order to evaluate the composition and chemical states of the produced oxide thin films, as well as their chemical composition. Spectra acquisition was done without flood gun, the carbonaceous contamination (C 1s binding Energy = 285 eV) being used as reference for binding energy correction. For quantitative data treatment, sensitivity factors provided by the equipment manufacturer were used.

The optical characteristics of the films were measured using a UV-VIS-IR spectrophotometer (3100 Shimadzu double beam) and a Jobin-Yvon UVISEL ellipsometer in the spectral range from 1 to 6 eV at an incidence angle of 70°. To determine the optical parameters of the films under analysis, we used a Tauc-Lorentz dispersion model with two oscillators. The electrical and optical properties of the oxide films produced were evaluated in 150-200 nm thick films, deposited on Corning 1737 glass substrates. The Ti/Au electrode patterns were obtained using shadow masks and their geometries are shown in the sketch of fig 1.c), for conductivity versus temperature (top) and Hall effect (bottom) measurements.

The I-V curves of the pn solar cells (Ag-Cr/p-c-Si/a-IZO/p-ZGO/Ag-Cr) were performed in the dark and under AM1.5 illumination using a Spire sun simulator. The electrical characterization of the transistors was performed using an Agilent 4155C semiconductor parameter analyzer and a Cascade Microtech M150 probe station. All the analyses were performed with a relative humidity of 35-40% and inside a dark box.

3. RESULTS

Before selecting the films for device fabrication, their structure, morphology and electro-optical characteristics were studied and related to the selected deposition parameters.

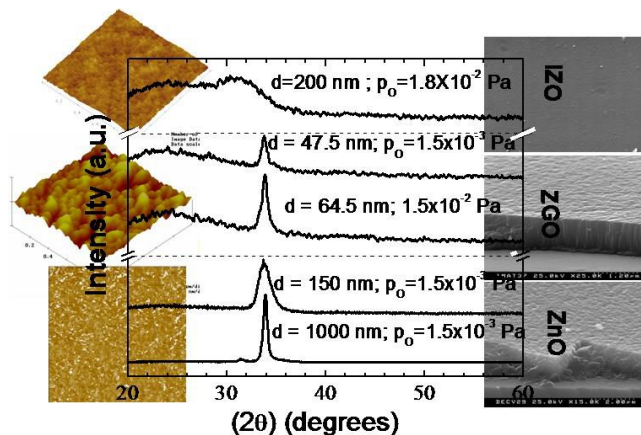


Fig. 2. XRD patterns of the a-IZO, poly-ZnO and poly-ZGO films. The labels indicate the film thickness and oxygen partial pressure used. The images on the left and right sides were obtained by AFM and SEM analysis, respectively.

Figure 2 shows the XRD patterns of the a-IZO, poly-ZnO and poly-ZGO films deposited on Corning substrates (center) and the corresponding surface morphology images obtained by AFM (left side) and SEM (right side). These films were used to fabricate the pn heterojunction solar cells and the poly-ZnO TFT.

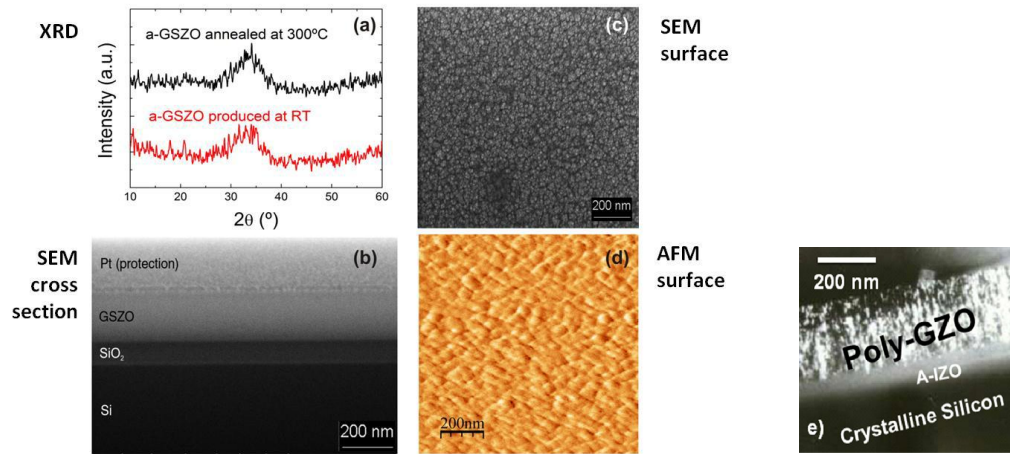


Fig. 3.a) XRD patterns of the a-ZGSO deposited at R.T. on a glass substrate, before and after annealing at 300 °C; b) SEM cross section of the ZGSO film deposited on a c-Si substrate coated with a thin SiO₂ layer, c) SEM surface image of the ZGSO film; d) AFM surface image of the same ZGSO film; e) SEM cross section of the p-c-Si/a-IZO/ZGO solar cell.

Figure 3 shows the XRD patterns (a), the SEM surface (c) and AFM (d) images of the ZGSO films used as semiconductor in TFTs. A SEM cross section (b and e) is also shown for two device structures (p-c-Si/SiO₂/a-ZGSO and p-c-Si/a-IZO/ZGO) used to fabricate TFTs and solar cells, respectively.

The composition of the ZGSO films was analyzed by XPS, for films that have sustained different annealing temperatures. The results achieved are depicted in Table 1.

Table 1. XPS atomic percentages for Ga, Zn, Sn and O elements and Ga/Zn and Sn/Zn atomic ratios

Annealing temperature	Ga	Zn	Sn	O (Oxide)	O (Hydroxide)	Ga/Zn	Sn/Zn
RT	1.6	24.6	6.6	35.5	31.7	0.07	0.27
200°C	1.6	24.6	7.2	40.4	26.2	0.07	0.29
300°C	2.5	21.2	11.8	45.5	19.2	0.12	0.56

The degree of films compactness and nature of the films structure were also analyzed by spectroscopic ellipsometry aiming to compare the behavior of the ZGO and ZGSO films. The results are depicted in fig.4 a) for the refractive index (n) and the extinction coefficient (k) as a function of the photon energy [52].

As far as the visible transmittance is concerned, all films exhibit transmittances above 75%, with the highest ones for the IZO films (87%). Also the optical band gap inferred from transmittance and spectroscopic ellipsometry data reveal that all films have an optical band gap above 3 eV.

The electrical properties of the films were also studied through the conductivity versus temperature and the Hall effect measurements. All films with $\rho < 10^{-3} \Omega \cdot \text{cm}$ are non-activated, as expected for degenerated oxide semiconductors [3]. For highly resistive films ($\rho > 10^{10} \Omega \cdot \text{cm}$), we could not determine the activation energy through the conductivity measurements, while for the so-called active oxide semiconductors (either polycrystalline or amorphous) this was accomplished, as shown for example in fig. 4b) for 300 °C annealed a-ZGSO films.

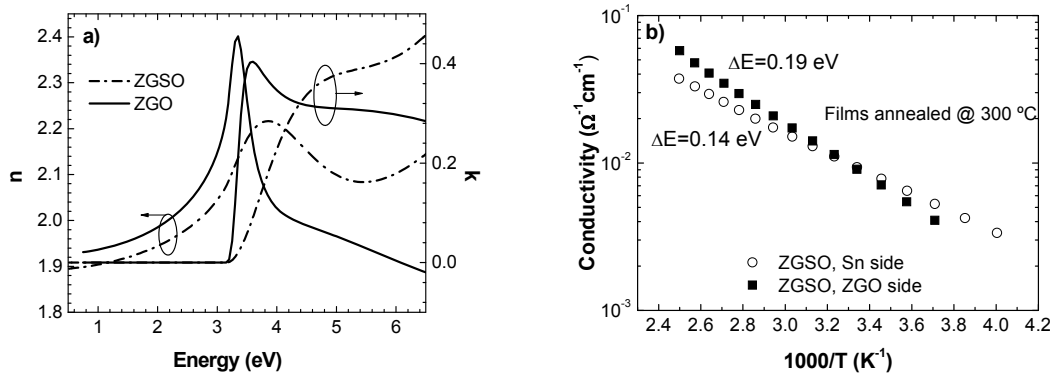


Fig. 4.a) Comparison of the refractive index (n) and the extinction coefficient (k) spectra of ZGO and ZGSO films obtained by spectroscopic ellipsometry; b) Arrhenius plot of the conductivity of a-ZGSO films with different Sn contents.

Table 2 also shows the Hall effect data concerning the ZnO, ZGO and ZGSO films used for the devices fabricated and studied along this work. There, we refer to the performance of films processed in different conditions: the ones grown above the Sn target are richer in Sn than the ones located close to the ZGO target (see fig.1).

Table 2. Electrical characteristics of the ZnO, ZGO and ZGSO films processed under different deposition conditions, before and after annealing.

<i>Sample/ target side</i>	<i>Resistivity (Ωcm)</i>	<i>Carrier mobility ($\text{cm}^2\text{V}^{-1}\text{s}^{-1}$)</i>	<i>Carrier concentration (cm^{-3})</i>
Poly-ZnO (a)	1.9×10^5	--	--
Poly-ZnO (b)	3.1×10^2	--	--
Poly-ZGO (a)	$(2-6) \times 10^{-4}$	10-18.5	$(1.65-9.85) \times 10^{20}$
ZGSO/Sn (a)	1.5×10^{10}	--	--
ZGSO/Sn (b)	9.4×10^1	5.5	1.2×10^{16}
ZGSO/ZGO (a)	8×10^{10}	--	--
ZGSO/ZGO (b)	5.2×10^1	4.7	3.1×10^{16}

(a) as deposited; (b) after annealing at 300 °C.

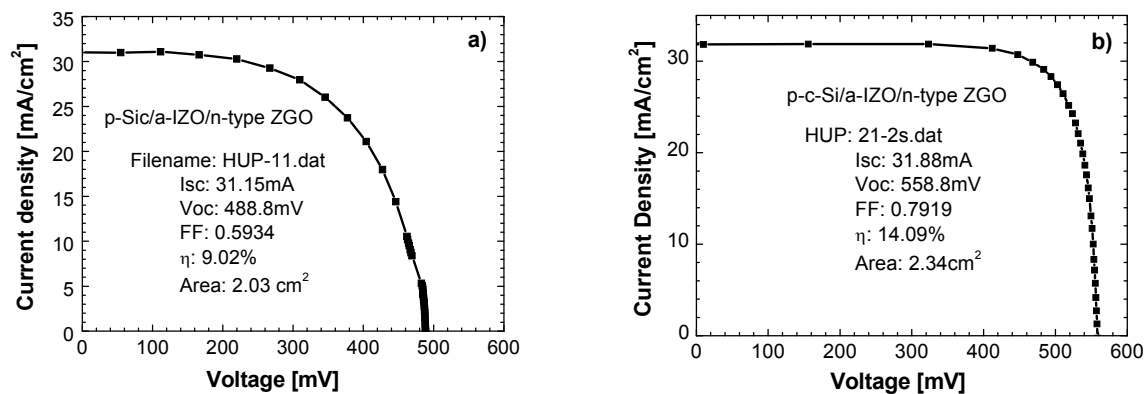


Fig. 5. I-V curves of the produced solar cells under AM1.5 illumination: a) p-c-Si/poly-ZGO; b) p-c-Si/a-IZO/poly-ZGO.

The I-V curves of the p-c-Si/Poly-ZGO and p-c-Si/a-IZO/Poly-ZGO solar cells taken under AM1.5 illumination are depicted in fig. 5. The resulting characterization parameters are presented inside each figure.

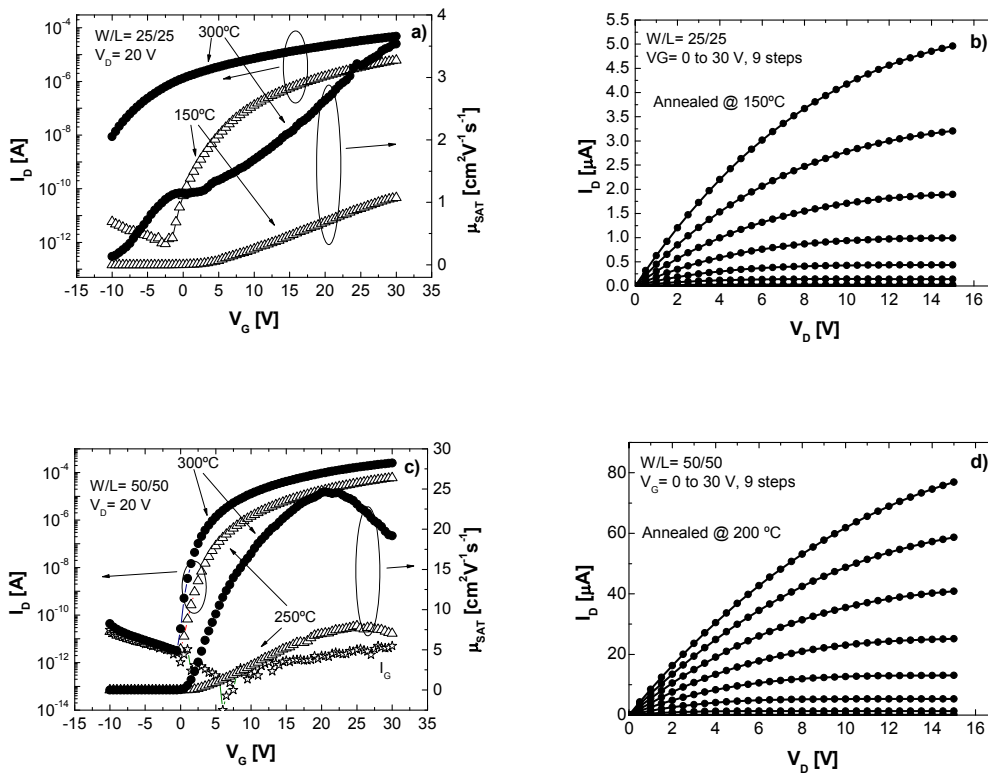


Fig. 6. Transfer and output characteristics of TFTs based on ZnO produced at R.T and a-ZGO produced at 150 °C: a) transfer characteristics for ZnO TFTs annealed at 150 and 300 °C; b) output characteristics for ZnO TFTs annealed at 150 °C; c) transfer characteristics for ZGO TFTs annealed at 250 and 300 °C; output characteristics for ZGO TFTs annealed at 200 °C.

The transfer and output characteristics of the n-type ZnO and a-ZGO TFTs are depicted in fig. 6, for films processed in the central region of the sputtering system (see fig. 1), at R.T. (ZnO) and 150 °C (a-ZGO S2). With a low temperature annealing (150 °C) the ZnO TFTs already present nice properties despite the low saturation mobility (μ_{SAT}), slightly higher than 1 cm²/Vs. μ_{SAT} is enhanced by annealing at 300 °C, however all the remaining properties are degraded (fig. 4 a and b). Concerning the a-ZGO based devices (fig. 6 c and d), channel conductivity modulation is negligible until the devices are annealed above 200 °C, and the properties are even improved at 300 °C.

The electrical characteristics of the ZnO and a-ZGO TFTs deposited at RT (S1) and 150 °C (S2) and annealed up to 300 °C are shown in Table 3.

Table 3. Electrical characteristics of the a-ZGO and poly-ZnO TFTs, as processed and after annealing.

	<i>a-ZGO S1 (R.T.)</i>			<i>a-ZGO S2 (150 °C)</i>			<i>Poly-ZnO (R.T.)</i>			
Annealing (°C)	a)	200	250	300	a)	200	250	300	150	300
μ_{SAT} (cm²/Vs)	nw	nw	7.9	18.1	ns	10.6	15.4	24.6	1.1*	3.5*
V_T (V)	nw	nw	6.5	6.5	ns	5.4	4.8	4.6	9.1	≈-3.3
I_{ON}/I_{OFF}	nw	nw	2×10 ⁷	6×10 ⁷	ns	3×10 ⁸	8×10 ⁷	8×10 ⁷	7×10 ⁶	>5×10 ³
S (V/decade)	nw	nw	0.75	0.62	ns	0.38	0.46	0.45	0.88	--

a) as-deposited; nw – not working; ns – not stable; * non-saturated value (V_G=30 V)

The transfer and output characteristics of the p-type TFT based on the Zn-Cu-O system (ZCO) after being annealed at 350 °C are depicted in fig. 7.

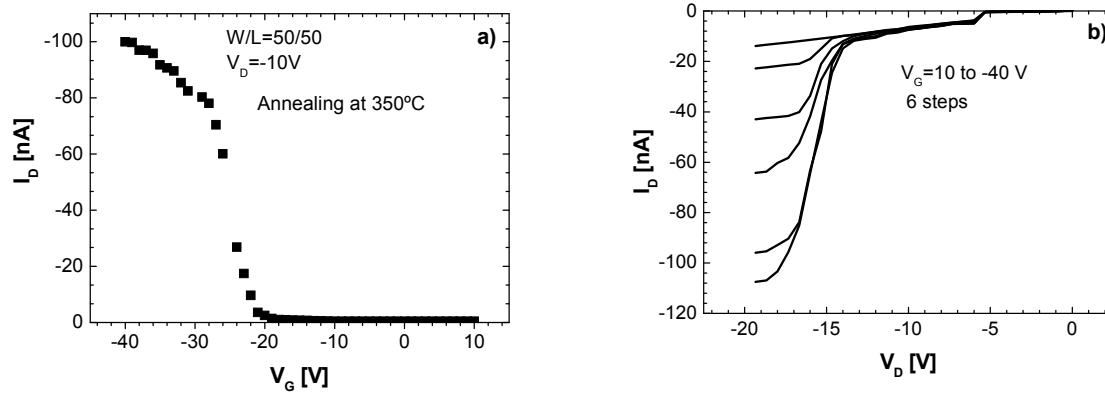


Fig. 7. Electrical performance of the ZCO TFT processed at 150 °C and annealed at 350 °C: a) transfer and b) output characteristics.

4. DISCUSSION OF THE RESULTS

4.1 Materials

Figures 2 and 3 show the structure and surface morphology of the IZO, ZGO and ZGSO films processed at room temperature. The data depicted show that the IZO films are amorphous exhibiting a smooth surface, with roughness below 0.5 nm. The film structure does not change after annealing at 250 °C. On the other hand, the ZGO films are polycrystalline with a preferred (0002) grain orientation and a roughness above 15-18 nm that is enhanced as the annealing temperature increases. This behavior is ascribed to the increase of the crystalline size^[14]. Similar results were found for ZnO. The XRD patterns (as produced and after being annealed at 300°C in a nitrogen atmosphere), AFM and SEM images reveal that the ZGSO films are amorphous, with a surface roughness below 0.7 nm.

Figure 4a) shows the refractive index and the extinction coefficient spectra for the poly-ZGO and a-ZGSO thin films depicted in fig. 2. The data show that near the band gap energy (3.6 eV) the poly-ZGO thin film exhibits a sharp peak associated to an abrupt variation of the extinction coefficient, which is attributed to the crystalline nature of the films, in line with the XRD data. On the other hand, the spectra of the a-ZGSO films exhibit a broad band whose peak is shifted to higher energies. This type of behavior is typical of amorphous structures^[56-58]. By comparing both films, the poly-ZGO has a higher refractive index in the transparent region than the a-ZGSO. Concerning the extinction coefficients, the a-ZGSO films present threshold energy higher than that of poly-ZGO. These results have also been observed for the case of a-GIZO thin films^[59].

In spite of the films' structure and morphology data do not show any detectable variation after annealing at 300 °C, the same does not occur to the electrical properties, especially for the a-ZGSO films, as can be seen in Table 2. The data reveal that as deposited (R.T.) poly-ZGO films are highly conductive ($\rho \approx 10^{-4} \Omega \cdot \text{cm}$), as desirable for applications as transparent conductive oxides. The same does not happen with the poly-ZnO and a-ZGSO films (rich or not in Sn), deposited at RT which are highly resistive (respectively higher than $10^5 \Omega \cdot \text{cm}$ and $10^{10} \Omega \cdot \text{cm}$). However, after annealing to 300 °C, the resistivity decreases by more than 3 order and 8 orders of magnitude, respectively for the poly-ZnO and a-ZGSO films. Besides that, after annealing the a-ZGSO films are activated, as shown by the Arrhenius plot in fig. 4b). The data show that the conductivity of Sn richer a-ZGSO films present an activation energy of 0.14 eV, while the ones with the lower Sn content exhibit an activation energy of 0.19 eV.

The decrease in resistivity with the annealing temperature is attributed to modification of the semiconductor and/or to the improved local atomic rearrangement, possibly related to a change in the oxidation state of Sn, from Sn_4^+ to Sn_2^+ . It is well known that Sn_2^+ absorbs at an energy range lower than Sn_4^+ , which explains the lower absorption coefficient observed for annealed a-ZGSO samples, as observed by Hosono et al^[60] in optical measurements performed to evaluate

the behavior of the absorption coefficient in a-ZGSO films. With increasing annealing temperature, there is a surface enrichment in Ga and especially in Sn.

This interpretation is reinforced by the XPS data shown in Table 1, for a-ZGSO films annealed up to 300 °C. The data show that as the annealing temperature increases up to 300 °C, the films' stoichiometry changes. The most noticeable changes are related to oxygen associated to oxide metal elements (which increases about 28.2%) or to hydroxide groups (which decreases about 39.4%). That is, ratio O(oxide)/O(hydroxide) increases with the annealing temperature, which could be related to oxygen adsorption from the environment and hydroxide groups. The Ga/Zn and Sn/Zn atomic ratio in as-deposited and 300 °C annealed samples reveal an enhancement of about 71.4% and 107.4%, respectively. These data clearly show that Sn changes its state of oxidation with the annealing process, leading to changes in the films' stoichiometry, involving Sn segregation towards the surface, with or without cations redistribution along the a-ZGSO thickness. Regarding photoelectron binding energy (B.E.) of different elements, they correspond to the oxidized forms B.E.(Ga 2p)=1118.7 ± 0.2 eV, typical of Ga 2p from Ga₂O₃ [61] and B.E.(Zn 2p)=1022.3 ± 0.2 eV, typical of Zn 2p from ZnO (see. NIST X-ray Photoelectron Spectroscopy Database, <http://srdata.nist.gov/xps/>, 2003). Concerning Sn, its photoelectrons Sn 3p and Sn 3d are present in all the samples, corresponding to binding energies of 716.1 ± 0.2 and 486.2 ± 0.2 eV, respectively. This can be assigned either to SnO or SnO₂, due to their binding energy proximity and the dispersion of values in literature. A more robust parameter, independent of charge accumulation correction, is the modified Auger parameter which is, for all the samples, 918.3 ± 0.2 eV which is closer to the SnO₂ modified Auger parameter than to the SnO one [62]. O 1s peak is fitted with two components centered at 530.4 ± 0.2 eV and at 532.1 ± 0.2 eV assignable, respectively to the oxide and hydroxide oxygen forms.

Another indirect result from XPS data concerns spectra charge shifts which were 9.5 eV, 8.5 eV and 4 eV for RT, 200 °C and 300 °C, respectively. This is an indication that the number of hole traps in the samples decrease with the annealing temperature. These results are directly related with the electrical properties exhibited by these films, where a tremendous improvement was observed, mainly for the carrier concentration.

4.2 Devices

Growing a ZGO film on silicon to form a heterojunction is potentially attractive for PV applications because such cells can have an excellent blue response (in contrast to many industrial c-Si solar cells which feature a heavily doped "dead" layer at the illuminated surface) and can be fabricated in a relatively simple way. The ITO/Si structure has been extensively studied during the past two decades by various deposition technologies. The conversion efficiencies achieved were 10-15% using spray pyrolysis [63], 9.8% using electron beam evaporation [64], and 12-16.5% using ion-beam sputtering [65]. However, little information is available in the literature on ZnO/c-Si heterojunction solar cells [66], and all the cells reported until now have a low energy conversion efficiency. In fig. 5 we present the electrical I-V curves under AM1.5 illumination of p-type c-Si/n-type poly-ZGO and p-type c-Si/a-IZO/n-type poly-ZGO heterojunction solar cells in a total active area of about 2 cm². The device without the a-IZO under layer (fig. 5a)) presents short circuit current density (J_{SC}), open circuit voltage (V_{OC}), fill factor (FF) and conversion efficiency (η) of 31.15 mAcm⁻², 488.8 mV, 0.59 and 9 %, respectively. For the device with the underneath a-IZO layer (fig. 5b)) the obtained properties are: J_{SC} = 31.88 mAcm⁻²; V_{OC} = 558.8 mV; FF = 0.79; η = 14.09 %. The data show an overall improvement on the solar cell performance above 56.6 % when the a-IZO intermediate layer is used. The most optimized device parameter is the FF (>33 %), followed by the V_{OC} (>14 %). This improvement could be related to a better matching promoted at the interface between the n-type poly-ZGO oxide and the p-type c-Si by the a-IZO, due to its work function and because the highly smooth surface of a-IZO films reduces the leakage current related to pinholes formation. This leads to an improvement of the shunt and series resistances of the device. No degradation of the cell efficiency was observed during a 50-hour illumination test (1 sun) and after storing the cell in air for six months.

Figure 6 and Table 3 show the transfer and output characteristics as well as the extracted electrical parameters of the n-type oxide TFTs analyzed in this work. In general, the data show that the performance of the amorphous TFTs is far better than the one of the poly-ZnO based devices. Besides that, the annealing treatment leads to electrical improvements on the amorphous oxide TFTs while the same does not occur to the polycrystalline oxide TFTs. Table 3 shows the results of a-ZGSO produced at R.T. (S1) and 150 °C (S2), before and after annealing. Note that for both series of a-ZGSO TFTs the non-annealed devices do not work properly, having always very low I_D even for V_G=40 V or 50 V and hence small channel conductivity modulation, being this even more significant for the S1 series. In fact, with the processing conditions used in this work, for maximum temperatures of 150 °C the best performance was obtained with poly-ZnO instead of a-ZGSO transistors.

The data in Table 3 show that the a-ZGSO TFT of S1 series start working properly only for annealing temperatures higher than 250 °C, while for the S2 TFT series, even though they work before annealing, the electrical behavior is not stable: for successive and repeated measurements a significant positive turn-on voltage (V_{on}) shift^[29] higher than 15 V is observed, which should be related with electron trapping close to the insulator-semiconductor interface. Only after annealing at 200 °C the S2 TFT series present stable and reproducible electrical characteristics. Concerning μ_{SAT} (calculated by the derivative of the $\sqrt{I_D}(V_G)$ plot with $V_D=20$ V) an increase is observed with the annealing temperature for both series of TFTs analyzed, with a maximum value in the order of 25 cm²/Vs, for a-ZGSO films processed with an initial temperature of 150 °C (S2). This improvement with annealing temperature is attributed to modification of the semiconductor/insulator interface with temperature and/or to improved local atomic rearrangement^[67] as it was confirmed by the XPS analysis. The threshold voltage (V_T) is generally lower for S2 than for S1 devices, around 5 and 6.5 V respectively, showing a trend to decrease as the annealing temperature increases. Again, this should be related with improved film and interface properties (for instance, lower density of traps or better atomic rearrangement, as already suggested above) when a-ZGSO is produced or annealed at higher temperatures. The I_{ON}/I_{OFF} ratio for both series of a-ZGSO TFTs is around 10⁷-10⁸, which is around 1 order of magnitude higher than the one obtained for the poly-ZnO TFTs. As can be seen from fig. 6, this difference is essentially related with differences in I_{ON} , since I_{OFF} is controlled by the SiO₂ leakage current.

Another significant difference between the presented poly-ZnO and a-ZGSO devices is the evolution of their μ_{SAT} values with V_G . For poly-ZnO, it can be seen that there is a trend to a continuous increase of μ_{SAT} while for a-ZGSO it saturates and starts to decrease for higher values of V_G (fig. 6 a) and c)). The trend verified for ZGSO is also typically found for a-GZO or other amorphous oxide semiconductors, being the decrease for higher V_G associated with the higher scattering that the electrons are subjected to as they move closer to the dielectric/semiconductor interface, which is reinforced by the higher scattering associated with the high V_D used (generally, for devices without contact problems, $\mu_{FE} > \mu_{SAT}$)^[29]. Nevertheless, even if not presented in fig. 6 a), in poly-ZnO TFTs the same μ_{SAT} evolution is visible if V_G is taken to higher values, like 80 V. Until $V_G=30$ V poly-ZnO TFT μ_{SAT} always increases due to the preponderance of the modulation of grain boundaries associated barriers as V_G increases, when compared to the scattering phenomena described above. Also due to these grain boundaries and to the higher roughness of poly-ZnO films, the maximum μ_{SAT} is considerably lower than the one obtained for a-ZGSO TFTs.

Besides the worst interface properties of SiO₂/ZnO, the higher values of subthreshold voltage swing (S) verified for poly-ZnO TFT can also be related with the presence of the grain boundaries barriers, which inhibit carrier transport, as opposed to the percolation conduction of the a-ZGSO through overlapping *s* orbitals. Besides that, S values are lower for 150 °C than R.T. produced a-ZGSO TFTs, which is again supported by the better interface and local atomic rearrangement of the films produced at higher temperature.

In fig. 7 we depict the preliminary electrical characteristics of p-type ZCO TFTs. The data reveal devices with I_{ON}/I_{OFF} ratio of about 10 and $\mu_{SAT} \approx 0.09$ cm² V⁻¹ s⁻¹. The observed behavior is attributed to the change of Cu oxidation state (from Cu⁺ to Cu²⁺)^[68], with some possible surface state passivation induced by N₂, after annealing the device in a N₂ atmosphere at 350 °C. This is still an open discussion that requires further work, aiming for a better understanding of the device behavior and the overall improvement of the electrical characteristics achieved.

5. CONCLUSIONS

In summary, we have demonstrated the possibility to produce high performance oxide based pn heterojunction solar cells and bottom gate TFTs using ordered and disordered semiconductors. Poly-ZGO proves to be an excellent candidate to fabricate solar cells with high efficiencies at very low cost, when compared to the traditional technologies. We observed a tremendous gain on the solar cell performance when an intermediate a-IZO layer is used between the p-type c-Si and the n-type poly-ZGO. The obtained solar cell characteristics are remarkable, specially the efficiency, which can be as high as 14 % in the entire active device area of 2.34 cm².

As far as the bottom gate poly-ZnO and a-ZGSO TFT are concerned, we observed a considerable improvement in the properties of devices based on a disordered channel layer material, after annealing up to 300 °C. The data show that the annealing treatment dominates device characteristics and minimizes the effect of other process parameters. The performance of the presented a-ZGSO TFT is comparable and in some cases superior to those of a-GIZO TFTs^[31]. This is a clear advantage since the replacement of In by Sn in the Ga-Zn-O system, is quite important due to the limited

availability of In. Apart from that, we also demonstrated the possibility to produce a p-type oxide TFT using the Zn-Cu-O system, whose results are quite encouraging for further activity.

ACKNOWLEDGEMENTS

This work was funded by the Portuguese Science Foundation (FCT-MCTES) through projects PTDC/CTM/23943/2006, PTDC/EEA-ELC/64975/2006. The authors would also like to thank Portuguese Science Foundation (FCT-MCTES) for the fellowships SFRH/BD/17970/2004 and SFRH/BD/27313/2006 given to two of the authors (Pedro Barquinha and Gonçalo Gonçalves). Thanks are also due to Ana M. Botelho do Rego from IST (Portugal) and Anna Vilà, from Barcelona University (Spain), for the XPS and EELS analyses performed.

REFERENCES

- [1] Ellmer, K., Klein, A., and Rech, B., [Transparent Conductive Zinc Oxide: Basics and Applications in Thin Film Solar Cells] Springer, Berlin (2008).
- [2] H.L. Hartnagel, A. L., Dawar, A.K. Jain, C Jagadish: , [Semiconducting Transparent Thin Films] Institute of Physics Publishing, Bristol (1995).
- [3] Tsuda, N., Nasu, K., Fujimori, A., and Sirtori, K., [Electronic Conduction in Oxides] Springer-Verlag, Berlin (2000).
- [4] Minami, T., "Transparent and conductive multicomponent oxide films prepared by magnetron sputtering," 45th National Symposium of the American-Vacuum-Society, 1765-1772 (1998).
- [5] Canhola, P., Martins, N., Raniero, L., Pereira, S., Fortunato, E., Ferreira, I., and Martins, R., "Role of annealing environment on the performances of large area ITO films produced by rf magnetron sputtering," 8th International Conference on Polycrystalline Semiconductors, 271-276 (2004).
- [6] Baia, I., Fernandes, B., Nunes, P., Quintela, M., and Martins, R., "Influence of the process parameters on structural and electrical properties of r.f. magnetron sputtering ITO films," 3rd Symposium O on Thin Film Materials for Large Area Electronics of the E-MRS 2000 Spring Meeting, 244-247 (2000).
- [7] Baia, I., Quintela, M., Mendes, L., Nunes, P., and Martins, R., "Performances exhibited by large area ITO layers produced by rf magnetron sputtering," Thin Solid Films, 337(1-2), 171-175 (1999).
- [8] Raniero, L., Ferreira, I., Pimentel, A., Goncalves, A., Canhola, P., Fortunato, E., and Martins, R., "Role of hydrogen plasma on electrical and optical properties of ZGO, ITO and IZO transparent and conductive coatings," Symposium on Thin Film and Nanostructured Materials for Photovoltaics held at the 2005 EMRS Meeting, 295-298 (2005).
- [9] Fortunato, E., Nunes, P., Marques, A., Costa, D., Aguas, H., Ferreira, I., Costa, M. E. V., and Martins, R., "Highly conductive/transparent ZnO : Al thin films deposited at room temperature by rf magnetron sputtering," Key Eng. Materials 230-2, 571-574 (2002).
- [10] Nunes, P., Fortunato, E., Tonello, P., Fernandes, F. B., Vilarinho, P., and Martins, R., "Effect of different dopant elements on the properties of ZnO thin films," VACUUM 64(3-4), 281-285 (2002).
- [11] Fortunato, E., Nunes, P., Costa, D., Brida, D., Ferreira, I., and Martins, R., "Characterization of aluminium doped zinc oxide thin films deposited on polymeric substrates," VACUUM 64(3-4), 233-236 (2002).
- [12] Nunes, P., Fortunato, E., Martins, R., and Vilarinho, P., "Properties presented by ZnO thin films deposited by magnetron sputtering and spray pyrolysis," Key Eng. Materials 230-2, 424-427 (2002).
- [13] Fortunato, E., Nunes, P., Marques, A., Costa, D., Aguas, H., Ferreira, I., Costa, M. E. V., and Martins, R., "Highly conductive/transparent ZnO : Al thin films deposited at room temperature by rf magnetron sputtering," Key Eng. Materials 230-2, 571-574 (2002).
- [14] Assuncao, V., Fortunato, E., Marques, A., Goncalves, A., Ferreira, I., Aguas, H., and Martins, R., "New challenges on gallium-doped zinc oxide films prepared by r.f. magnetron sputtering," Thin Solid Films, 102-106 (2003).
- [15] Fortunato, E., Raniero, L., Silva, L., Goncalves, A., Pimentel, A., Barquinha, P., Aguas, H., Pereira, L., Goncalves, G., Ferreira, I., Elangovan, E., and Martins, R., "Highly stable transparent and conducting gallium-doped zinc oxide thin films for photovoltaic applications," Solar Energy Materials and Solar Cells, 92(12), 1605-1610 (2008).

- [16] Martins, R., Barquinha, P., Pimentel, A., Pereira, L., and Fortunato, E., "Transport in high mobility amorphous wide band gap indium zinc oxide films," *Physica Status Solidi a-Applications and Materials Science*, 202(9), R95-R97 (2005).
- [17] Martins, R., Barquinha, P., Pimentel, A., Pereira, L., Fortunato, E., Kang, D., Song, I., Kim, C., Park, J., and Park, Y., "Electron transport in single and multicomponent n-type oxide semiconductors," *Thin Solid Films*, 516 (7), 1322-1325 (2008).
- [18] Bae, H. S., Yoon, M. H., Kim, J. H., and Im, S., "Photodetecting properties of ZnO-based thin-film transistors," *Applied Physics Letters*, 83(25), 5313-5315 (2003).
- [19] Nomura, K., Ohta, H., Ueda, K., Kamiya, T., Hirano, M., and Hosono, H., "Thin-film transistor fabricated in single-crystalline transparent oxide semiconductor," *Science*, 300(5623), 1269-1272 (2003).
- [20] Wager, J. F., "Transparent electronics," *Science*, 300(5623), 1245-1246 (2003).
- [21] Fortunato, E., Pimentel, A., Pereira, L., Goncalves, A., Lavareda, G., Aguas, H., Ferreira, I., Carvalho, C. N., and Martins, R., "High field-effect mobility zinc oxide thin film transistors produced at room temperature," 20th International Conference on Amorphous and Microcrystalline Semiconductors, 806-809 (2003).
- [22] Fortunato, E. M. C., Barquinha, P. M. C., Pimentel, A., Goncalves, A. M. F., Marques, A. J. S., Martins, R. F. P., and Pereira, L. M. N., "Wide-bandgap high-mobility ZnO thin-film transistors produced at room temperature," *Applied Physics Letters*, 85(13), 2541-2543 (2004).
- [23] Martins, R., Barquinha, P., Pereira, L., Correia, N., Goncalves, G., Ferreira, I., and Fortunato, E., "Write-erase and read paper memory transistor," *Applied Physics Letters*, 93(20), (2008).
- [24] Fortunato, E., Correia, N., Barquinha, P., Pereira, L., Goncalves, G., and Martins, R., "High-performance flexible hybrid field-effect transistors based on cellulose fiber paper," *Ieee Electron Device Letters*, 29(9), 988-990 (2008).
- [25] Carcia, P. F., McLean, R. S., and Reilly, M. H., "Oxide engineering of ZnO thin-film transistors for flexible electronics," *Journal of the Society for Information Display*, 13(7), 547-554 (2005).
- [26] Carcia, P. F., McLean, R. S., and Reilly, M. H., "High-performance ZnO thin-film transistors on gate dielectrics grown by atomic layer deposition," *Applied Physics Letters*, 88(12), (2006).
- [27] Carcia, P. F., McLean, R. S., Reilly, M. H., Malajovich, I., Sharp, K. G., Agrawal, S., and Nunes, G., "ZnO thin film transistors for flexible electronics," Symposium on Flexible Electronics-Materials and Device Technology held at the 2003 MRS Spring Meeting, 233-238 (2003).
- [28] Martins, R., Fortunato, E., Nunes, P., Ferreira, I., Marques, A., Bender, M., Katsarakis, N., Cimalla, V., and Kiriakidis, G., "Zinc oxide as an ozone sensor," *Journal of Applied Physics*, 96(3), 1398-1408 (2004).
- [29] Barquinha, P., Pereira, L., Goncalves, G., Martins, R., and E., F., "Toward High-Performance Amorphous GIZO TFTs," *J. Electrochem. Soc.*, 156(3), H161-H168 (2009).
- [30] Barquinha, P., Vila, A., Goncalves, G., Pereira, L., Martins, R., Morante, J., and Fortunato, E., "The role of source and drain material in the performance of GIZO based thin-film transistors," E-MRS 2007 Spring Meeting Symposium on Advances in Transparent Electronics: From Materials to Devices II, 1905-1909 (2007).
- [31] Barquinha, P., Vila, A. M., Goncalves, G., Martins, R., Morante, J. R., Fortunato, E., and Pereira, L., "Gallium-indium-zinc-oxide-based thin-film transistors: Influence of the source/drain material," *Ieee Transactions on Electron Devices*, 55(4), 954-960 (2008).
- [32] Chiang, H. Q., McFarlane, B. R., Hong, D., Presley, R. E., and Wager, J. F., "Processing effects on the stability of amorphous indium gallium zinc oxide thin-film transistors," 22nd International Conference on Amorphous and Nanocrystalline Semiconductors, 2826-2830 (2007).
- [33] Chuang, C. S., Fung, T. C., Mullins, B. G., Nomura, K., Kamiya, T., Shieh, H. P. D., Hosono, H., and Kanicki, J., "Photosensitivity of amorphous IGZO TFTs for active-matrix flat-panel displays," International Symposium of the Society-for-Information-Display (SID 2008), 1215-1218 (2008).
- [34] Hong, D., Yerubandi, G., Chiang, H. Q., Spiegelberg, M. C., and Wager, J. F., "Electrical modeling of thin-film transistors," *Critical Reviews in Solid State and Materials Sciences*, 33(2), 101-132 (2008).
- [35] Noborio, M., Suda, J., and Kimoto, T., "N₂O-grown oxides/4H-SiC (0001), (0338), and (1120) interface properties characterized by using p-type gate-controlled diodes," *Applied Physics Letters*, 93(19), (2008).
- [36] Ohta, H., Sugiura, K., and Koumoto, K., "Recent progress in oxide thermoelectric materials: p-type Ca₃Co₄O₉ and n-type SrTiO₃," *Inorganic Chemistry*, 47(19), 8429-8436 (2008).
- [37] Look, D., "Donors and acceptors in bulk ZnO grown by the hydrothermal, vapor-phase, and melt processes," Symposium on Zinc Oxide and Related Materials held at the 2006 MRS Fall Meeting, 127-133 (2006).

- [38] Tsuboi, N., Hoshino, T., Kobayashi, S., Kato, K., and Kaneko, F., "P-type conductive CuYO₂ phosphor co-doped with Eu, Tb or Tm rare-earth cation and Ca acceptor cation," *Physica Status Solidi a-Applications and Materials Science*, 203(11), 2723-2728 (2006).
- [39] Nakaoka, K., and Ogura, K., "Electrochemical preparation of p-type cupric and cuprous oxides on platinum and gold substrates from copper(II) solutions with various amino acids," *Journal of the Electrochemical Society*, 149(11), C579-C585 (2002).
- [40] Kawazoe, H., Yanagi, H., Ueda, K., and Hosono, H., "Transparent p-type conducting oxides: Design and fabrication of p-n heterojunctions," *Mrs Bulletin*, 25(8), 28-36 (2000).
- [41] Watanabe, A., "Highly conductive oxides, CeVO₄, Ce_{1-x}M_xVO_{4-0.5x}(M= Ca, Sr, Pb) and Ce_{1-y}Bi_yVO₄, with zircon-type structure prepared by solid-state reaction in air," *Journal of Solid State Chemistry*, 153(1), 174-179 (2000).
- [42] Kudo, A., Yanagi, H., Ueda, K., Hosono, H., Kawazoe, H., and Yano, Y., "Fabrication of transparent p-n heterojunction thin film diodes based entirely on oxide semiconductors," *Applied Physics Letters*, 75(18), 2851-2853 (1999).
- [43] Kawazoe, H., Yasukawa, M., Hyodo, H., Kurita, M., Yanagi, H., and Hosono, H., "P-type electrical conduction in transparent thin films of CuAlO₂," *Nature*, 389(6654), 939-942 (1997).
- [44] Ogo, Y., Hiramatsu, H., Nomura, K., Yanagi, H., Kamiya, T., Hirano, M., and Hosono, H., "p-channel thin-film transistor using p-type oxide semiconductor, SnO," *Applied Physics Letters*, 93(3), (2008).
- [45] Böer, K. W., [Survey in Semiconductor Physics, Electrons and Other Particles in Bulk Semiconductors] Van Nostrand Reinhold, New York (1990).
- [46] Martins, R., Barquinha, P., Pereira, L., Ferreira, I., and Fortunato, E., "Role of order and disorder in covalent semiconductors and ionic oxides used to produce thin film transistors," *Applied Physics a-Materials Science & Processing*, 89(1), 37-42 (2007).
- [47] Martins, R., Baptista, P., Raniero, L., Doria, G., Silva, L., Franco, R., and Fortunato, E., "Amorphous/nanocrystalline silicon biosensor for the specific identification of unamplified nucleic acid sequences using gold nanoparticle probes," *Applied Physics Letters*, 90(2), (2007).
- [48] Shur, M., [Physics of Semiconductor Devices] Prentice Hill, New Jersey, USA (1990).
- [49] Street, R. A., [Technology and Applications of Amorphous Semiconductors] Springer, Berlin (2000).
- [50] Robertson, J., "Disorder and instability processes in amorphous conducting oxides," *Physica Status Solidi B-Basic Solid State Physics*, 245(6), 1026-1032 (2008).
- [51] Hosono, H., Nomura, K., Ogo, Y., Uruga, T., and Kamiya, T., "Factors controlling electron transport properties in transparent amorphous oxide semiconductors," 22nd International Conference on Amorphous and Nanocrystalline Semiconductors, 2796-2800 (2007).
- [52] Martins, R., Barquinha, P., Ferreira, I., Pereira, L., Goncalves, G., and Fortunato, E., "Role of order and disorder on the electronic performances of oxide semiconductor thin film transistors," *Journal of Applied Physics*, 101(4), (2007).
- [53] Fortunato, E. M. C., Pereira, L. M. N., Barquinha, P. M. C., do Rego, A. M. B., Goncalves, G., Vila, A., Morante, J. R., and Martins, R. F. P., "High mobility indium free amorphous oxide thin film transistors," *Applied Physics Letters*, 92(22), (2008).
- [54] Fortunato, E., Barquinha, P., Pimentel, A., Pereira, L., Goncalves, G., and Martins, R., "Amorphous IZO TTFTs with saturation mobilities exceeding 100 cm²/Vs," *Physica Status Solidi-Rapid Research Letters*, 1(1), R34-R36 (2007).
- [55] Martins, R., Almeida, P., Barquinha, P., Pereira, L., Pimentel, A., Ferreira, I., and Fortunato, E., "Electron transport and optical characteristics in amorphous indium zinc oxide films," *Journal of non-Cryst. Solids* 352 (9-20), 1471-1474 (2006).
- [56] Aguas, H., Popovici, N., Pereira, L., Conde, O., Branford, W. R., Cohen, L. F., Fortunato, E., and Martins, R., "Spectroscopic ellipsometry study of Co-doped TiO₂ films," *Physica Status Solidi a-Applications and Materials Science*, 205(4), 880-883 (2008).
- [57] Pereira, L., Aguas, H., Beckers, M., Martins, R. M. S., Fortunato, E., and Martins, R., "Spectroscopic ellipsometry study of nickel induced crystallization of a-Si," 21st International Conference on Amorphous and Nanocrystalline Semiconductors, 1204-1208 (2005).
- [58] Martins, R., Aguas, H., Ferreira, I., Fortunato, E., Lebib, S., Cabarrocas, P. R. I., and Guimaraes, L., "Polymorphous silicon films deposited at 27.12 MHz," *Chemical Vapor Deposition*, 9(6), 333-337 (2003).

- [59] Kang, D., Song, I., Kim, C., Park, Y., Kang, T. D., Lee, H. S., Park, J. W., Baek, S. H., Choi, S. H., and Lee, H., "Effect of Ga/In ratio on the optical and electrical properties of GaInZnO thin films grown on SiO₂/Si substrates," *Applied Physics Letters*, 91(9), (2007).
- [60] Hosono, H., Nomura, K., Ogo, Y., Uruga, T., and Kamiya, T., "Factors controlling electron transport properties in transparent amorphous oxide semiconductors," *J. Non-Cryst. Solids* 354(19-25), 2796-2800 (2008).
- [61] Vilar, M. R., El Beghdadi, J., Debontridder, F., Artzi, R., Naaman, R., Ferrara, A. M., and do Rego, A. M. B., "Characterization of wet-etched GaAs (100) surfaces," *Surface and Interface Analysis*, 37(8), 673-682 (2005).
- [62] Jimenez, V. M., Mejias, J. A., Espinos, J. P., and GonzalezElipse, A. R., "Interface effects for metal oxide thin films deposited on another metal oxide .2. SnO₂ deposited on SiO₂," *Surface Science*, 366(3), 545-555 (1996).
- [63] Manificier, J. C., and Szepessy, L., "EFFICIENT SPRAYED IN₂O₃-SN N-TYPE SILICON HETEROJUNCTION SOLAR-CELL," *Applied Physics Letters*, 31(7), 459-462 (1977).
- [64] Feng, T., Ghosh, A. K., and Fishman, C., "EFFICIENT ELECTRON-BEAM-DEPOSITED ITO-N-SI SOLAR-CELLS," *Journal of Applied Physics*, 50(7), 4972-4974 (1979).
- [65] Dubow, J. B., Burk, D. E., and Sites, J. R., "EFFICIENT PHOTOVOLTAIC HETEROJUNCTIONS OF INDIUM TIN OXIDES ON SILICON," *Applied Physics Letters*, 29(8), 494-496 (1976).
- [66] Kobayashi, H., Mori, H., Ishida, T., and Nakato, Y., "ZINC-OXIDE N-SI JUNCTION SOLAR-CELLS PRODUCED BY SPRAY-PYROLYSIS METHOD," *Journal of Applied Physics*, 77(3), 1301-1307 (1995).
- [67] Chiang, H. Q., Wager, J. F., Hoffman, R. L., Jeong, J., and Keszler, D. A., "High mobility transparent thin-film transistors with amorphous zinc tin oxide channel layer," *Applied Physics Letters*, 86(1), (2005).
- [68] Figueiredo, V., Elangovan, E., Goncalves, G., Barquinha, P., Pereira, L., Franco, N., Alves, E., Martins, R., and Fortunato, E., "Effect of post-annealing on the properties of copper oxide thin films obtained from the oxidation of evaporated metallic copper," *Applied Surface Science*, 254(13), 3949-3954 (2008).